Front. Chem. Sci. Eng. 2022, 16(1): 112–120
https://doi.org/10.1007/s11705-021-2075-5

RESEARCH ARTICLE

Novel lysosome-targeted anticancer fluorescent agents used in zebrafish and nude mouse tumour imaging

Xiuli Chen[1,2*], Feng Liu[1*], Bin Chen[3*], Haiying Wu[2], Kun Li[1], Yongmei Xie[1], Weihong Kuang (✉)[4], Zhihui Li (✉)[1,3]

1 Department of Thyroid Surgery, West China Hospital of Sichuan University, Chengdu 610041, China
2 Department of Obstetrics, Henan Provincial People's Hospital, People's Hospital of Zhengzhou University, Zhengzhou 450003, China
3 Laboratory of Thyroid and Parathyroid Disease, Frontiers Science Center for Disease-related Molecular Network, Rare Diseases Center, West China Hospital of Sichuan University, Chengdu 610041, China
4 Department of Psychiatry and National Clinical Research Center for Geriatrics, West China Hospital, Sichuan University, Chengdu 610041, China

Abstract The design of three novel fatty nitrogen mustard-based anticancer agents with fluorophores incorporated into the alkene structure (**CXL 118**, **CXL121**, and **CXL122**) is described in this report. The results indicated that these compounds are selectively located in lysosomes and exhibit effective antitumour activity. Notably, these compounds can directly serve as both reporting and imaging agents *in vitro* and *in vivo* without the need to add other fluorescent tagging agents.

Keywords fluorescent drug, lysosomal, anticancer, zebrafish, nude-mouse tumour imaging

1 Introduction

Lysosomes, existing in all protozoa and multicellular animal cells, are essential organelles that degrade endocytosed poisonous molecules. Because they contain a wide spectrum of hydrolytic enzymes, lysosomes play major roles in the degradation and recycling of macromolecules [1–4]. Lysosome dysfunction is often involved in pathologies, including cancer [5], neurodegenerative diseases [6–8], atherosclerosis, and rheumatoid arthritis [9,10]. Recently, researchers have shown great interest in lysosome research and have achieved certain scientific results. Miao et al. demonstrated that the activation of lysosomes is induced by structural damage and the role of this activation pathway in extracellular matrix regeneration [11]. Fujimaki et al. revealed for the first time that lysosomal function plays an important role as a "regulatory switch" in mediating the extent eukaryotic cells quiescence [12]. These research results are of great significance for understanding important physiological processes such as tissue homeostasis, repair and regeneration and ageing of the body. In terms of fluorescent probes, Hu et al. designed a new type of fluorescent molecule that is sensitive to intracellular polarity [13]. The probe emits red and blue light in lysosomes with high polarity and lipids with low polarity, respectively. The study of Hu et al. provided a new idea for studying the mechanism of lipid droplet-lysosome interactions and related diseases. In addition, lysosomes are involved in many cell signalling pathways, e.g., endocytosis, autophagy, and apoptosis [2,14,15], and many lysosomal proteases, such as cathepsins and lysosome-associated membrane glycoprotein (Lamp) signalling pathways, are involved in apoptosis [16]. Werneburg et al. reported that a tumour necrosis factor-related apoptosis-inducing ligand activates a lysosomal pathway of apoptosis that is regulated by bcl-2 proteins [17]. These studies show that the visualization of lysosomes is critical for understanding intracellular metabolism and cell membrane recycling [18,19]. Therefore, development of lysosomal-targeted fluorescent probes is a useful endeavour.

Cell death in mammals can be characterized by two main types: apoptosis and necrosis [20–22]. Autophagy, which has recently been proposed as a third distinct mode of cell death, is a homeostatic process critical for sequestering long-lived proteins and damaged organelles for subsequent degradation upon fusion with a lysosome [20,23–25]. Autophagy and apoptosis are activated in parallel in

Received December 31, 2020; accepted May 27, 2021

E-mails: kwhhlj@scu.edu.cn (Kuang W),
Rockoliver163@163.com (Li Z)

*These authors contributed equally to this work

cancer. In addition, autophagy plays a complex role in cancer [5,26,27].

Nitrogen mustards (*N*-mustards) are dichloroethylamine alkylating agents and are highly active compounds. These compounds possess an active group, bis(2-chloroethyl) amine, which can interact with amino, sulfhydryl, carboxyl and phosphoric acids in cells [28–30]. The reactions eventually affect the metabolism of cells and lead to cell death. However, drawbacks to the use of *N*-mustards to promote cell death include poor selectivity in the intracellular milieu and reactivity with untargeted cellular components, which may result in many unwanted side effects, such as bone marrow toxicity and genotoxicity [31]. Therefore, over decades, many structural modifications have been made to the *N*-mustard scaffold to increase its targeting affinity/specificity. Most modifications of *N*-mustard compounds are directed to the carrier structure [32]. Compared with other types of *N*-mustards, the nitrogen atom in fatty *N*-mustard is more alkaline. Thus, in free fatty nitrogen mustard and fatty nitrogen mustard at physiological pH values, the nitrogen atom is more likely to cause intramolecular cyclization, resulting in the formation of ethyleneimine ions, which are highly active strong electrophilic alkylating agents [33,34]. As a consequence, fatty *N*-mustards have great potential for high antitumour activity in a wide range of *in vitro* and *in vivo* environments [35].

To our knowledge, most fluorescent probes, which are powerful tools used in cell biology, cannot simultaneously meet the two requirements for effective visualization and antitumour activity. Recently, our group presented several new types of mitochondria-targeting *N*-mustard agents with fluorophores incorporated into the main *N*-mustard skeleton [36–39]. The molecules we synthesized exhibited highly selective activity against cancer cells. In biology and life sciences, the development of lysosome-targeting *N*-mustard fluorescent drugs is important for lysosome imaging and the treatment of lysosome-related diseases. In previous works, we have reported two new types of molecules, both aromatic *N*-mustards, with mitochondria-targeting imaging and fluorescent DNA alkylation ability [36,37]. In the present study, when we replaced aromatic *N*-mustard with fatty *N*-mustard, three lysosome-targeted agents (**CXL118**, **CXL121**, and **CXL122**) were formed, and then, three different fluorophores were integrated into the fatty *N*-mustard skeleton. As shown in Fig. 1, fluorophores 2-(2-methyl-4H-chromen-4-ylidene)malononitrile, 1-ethyl-2,3,3-trimethyl-3H-indol-1-ium, and 3-ethyl-1,1,2-trimethyl-1H-benzoindol-3-ium were linked to fatty *N*-mustard skeletons by an olefin double bond. Our synthetic probes were then used for zebrafish and nude mouse tumour imaging. The experiments showed that these probes can be used for diagnostic imaging.

2 Experimental

2.1 Materials and methods

All reagents are purchased with no special note. All of the solvents were dried according to the standard methods and were spectroscopic grade in the optical spectroscopic studies. Nuclear magnetic resonance (NMR) spectra were measured on a Bruker AM-400. The ^{1}H NMR (400 MHz) and ^{13}C NMR (101 MHz) chemical shifts were given using $CDCl_3$ and DMSO-d_6 as the internal standard. The ^{1}H NMR (400 MHz) chemical shifts were given in ppm relative to the internal reference trimethylchlorosilane. Electro-spray ionization mass spectral and high-resolution mass spectral data were recorded on a Finnigan LCQDECA and a Bruker Daltonics Bio TOF mass spectrometer, respectively. JUNYI Power Supply of JY300C was used for DNA agarose gel electrophoresis, data recorded in the Molecular Imager of Gel Doc TM XR+ with Image Lab TM Software of BIO-RAD. Inhibition rate is calculated by software of Graph Pad Prism 5.01 (Graph Pad Software, USA).

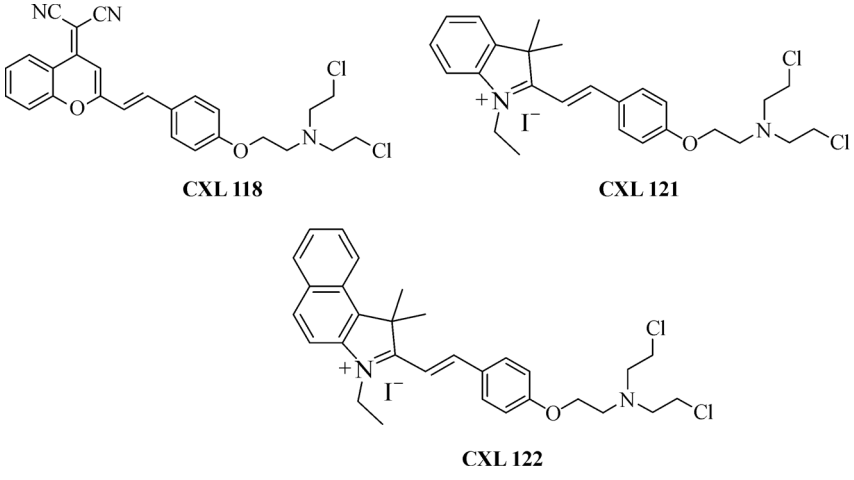

Fig. 1 Novel functional fluorescence compounds developed in this study.

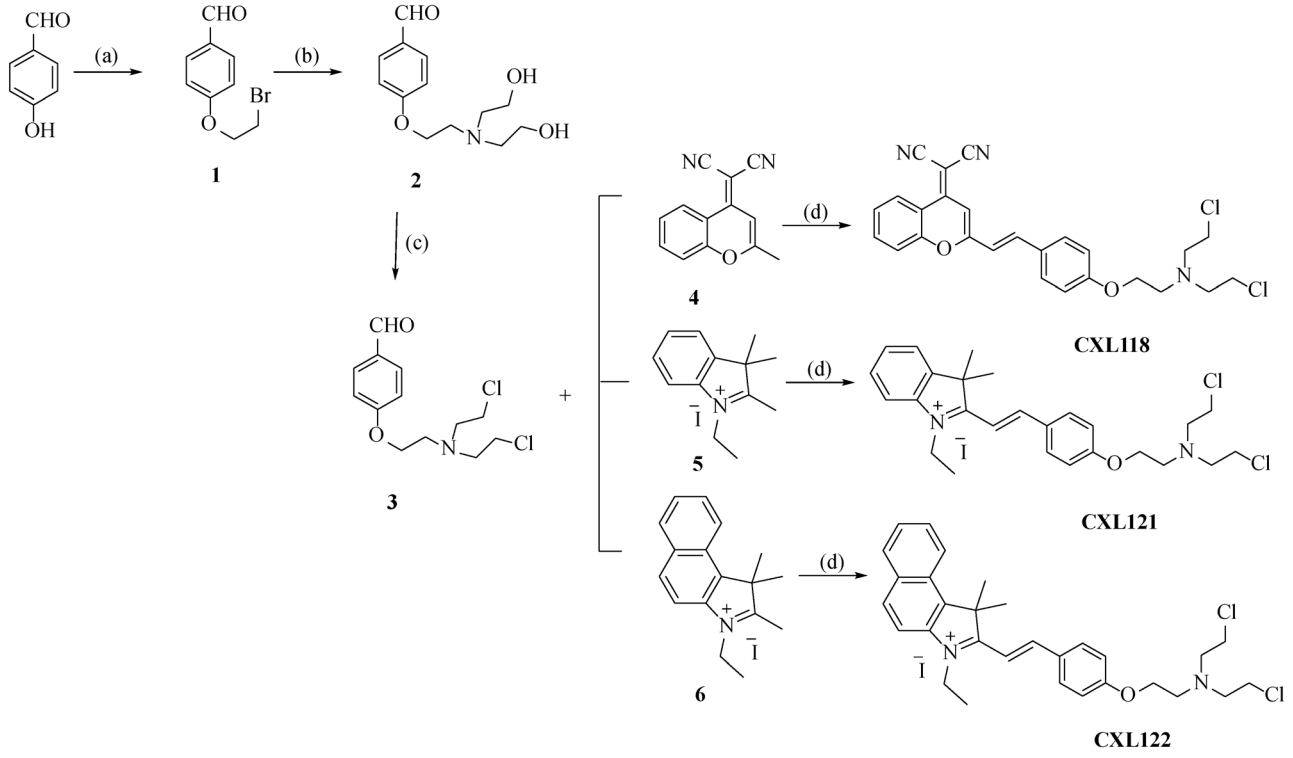

Scheme 1 Synthetic routes of compounds **CXL118**, **CXL121**, and **CXL122**. (a) 1,2-dibromoethane, K_2CO_3, DMF, 80 °C; (b) K_2CO_3, acetonitrile, 80 °C, (c) $SOCl_2$, DCM, 30 °C, and (d) piperidine, acetonitrile, 60 °C.

2.2 Synthesis and characterization of compounds **CXL118**, **CXL121**, and **CXL122**

The synthetic procedures of probes were depicted in Scheme 1. All the designed compounds contain two parts that are chromophoric units and *N*-mustards "warhead". Initially, the intermediates of chromophoric units **4**, **5**, and **6** and *N*-mustards "warhead" including 4-(2-(bis(2-chloroethyl)amino)ethoxy)benzaldehyde (**3**) were synthesized. Take the case of compound synthesis process of **CXL118**.

General process: 2-(2-Methyl-4H-chromen-4-ylidene) malononitrile (**4**) (208 mg, 1 mmol) and 4-(2-(bis(2-chloroethyl)amino)ethoxy)benzaldehyde (**3**) (289 mg, 1 mmol) were dissolved in dry acetonitrile (100 mL for 14 mmol) under argon. Piperidine (91 μL, 1 mmol) was added and the solution was stirred at 60 °C for 8 h. The red solution was concentrated and the product (**CXL118**, (E)-2-(2-(4-(2-(bis(2-chloroethyl)amino)ethoxy)styryl)-4H-chromen-4-ylidene)malononitrile) was purified by crystallization or column chromatography. Brick red solid; Yield 26%. ^{1}H NMR (400 MHz, $CDCl_3$, δ_{ppm}): 8.93 (t, J = 12.4 Hz, 1H, Ar–H), 7.75 (t, J = 8.2 Hz, 1H, Ar–H), 7.58–7.56 (m, 4H, Ar–H), 7.45 (t, J = 4.2 Hz, 1H, Ar–H), 6.96 (d, J = 8.4 Hz, 2H, –CH = CH–), 6.85 (s, 1H, Ar–H), 6.69 (d, J = 8.6 Hz, 1H, Ar–H), 4.10 (t, J = 6.4 Hz, 2H, –O–CH_2–CH_2–), 3.56 (t, J = 6.2 Hz, 4H, $N(CH_2)_2$), 3.10–3.03 (m, 4H, –CH_2Cl), 2.02 (m, 2H, –O–CH_2–CH_2–). ^{13}C NMR (101 MHz, DMSO, δ_{ppm}): 159.08, 153.37, 152.50, 139.13, 135.81, 130.56, 126.57, 125.10, 119.49, 117.56, 116.43, 115.60, 106.54, 60.00, 56.58, 53.03. MS *m/z* (ESI): calcd for $C_{26}H_{24}Cl_2N_3O_2^+$: 480.12; found 480.13.

(E)-2-(4-(2-(Bis(2-chloroethyl)amino)ethoxy)styryl)-1-ethyl-3,3-dimethyl-3H-indol-1-ium (**CXL121**): Yield 23%. ^{1}H NMR (400 MHz, $CDCl_3$, δ_{ppm}): 8.30 (t, J = 8.6 Hz, 2H, Ar–H), 8.22 (d, J = 8.2 Hz, 1H, Ar–H), 7.56 (d, J = 10.4 Hz, 1H, Ar–H), 7.57–7.50 (m, 4H, Ar–H), 7.06 (t, J = 10.6 Hz, 2H, –CH = CH–), 5.05–5.00 (q, J = 14.4 Hz, 7.2 Hz, 2H, –NCH_2CH_3), 4.15 (t, J = 6.4 Hz, 2H, –O–CH_2–CH_2–), 3.52 (t, J = 8.6 Hz, 3H, –CH_2Cl), 3.25–3.19 (m, 1H, –CH_2Cl), 3.18–2.99 (m, 6H, $N(CH_2)_3$), 1.84 (s, 6H, –$(CH_3)_2$), 1.62 (t, J = 6.8 Hz, 3H, –CH_2–CH_3). ^{13}C NMR (101 MHz, DMSO, δ_{ppm}): 181.70, 162.16, 154.21, 153.84, 144.26, 140.90, 133.67, 130.10, 129.56, 128.61, 123.57, 116.22, 115.41, 110.95, 55.91, 52.58, 51.75, 28.81, 26.23, 22.53, 14.15. MS *m/z* (ESI): calcd for $C_{26}H_{33}Cl_2N_2O^+$: 459.19; found 459.19.

(E)-2-(4-(2-(Bis(2-chloroethyl)amino)ethoxy)styryl)-3-ethyl-1,1-dimethyl-1H-benzo[e]indol-3-ium (**CXL122**): Yield 19%. ^{1}H NMR (400 MHz, $CDCl_3$, δ_{ppm}): 8.32–8.19 (m, 4H, Ar–H), 8.12 (d, J = 8.6 Hz, 1H, Ar–H), 8.07 (t, J = 10.6 Hz, 1H, Ar–H), 7.84 (t, J = 8.4 Hz, 1H, Ar–H), 7.77–7.71 (m, 2H, Ar–H), 7.67 (t, J = 8.0 Hz, 1H, Ar–H),

7.09 (dd, J = 12.4 Hz, 8.2 Hz, 2H, –CH = CH–), 5.17 (q, J = 10.6 Hz, 8.4 Hz, 2H, $–NCH_2CH_3$), 4.16 (t, J = 8.8 Hz, 2H, $–O–CH_2–CH_2–$), 3.56 (t, J = 4.8 Hz, 3H, $–CH_2Cl$), 3.19 (t, J = 12.0 Hz, 1H, $–CH_2Cl$), 3.12–3.01 (m, 6H, N $(CH_2)_3$), 2.10 (s, 6H, $–(CH_3)_2$), 1.69 (t, J = 8.2 Hz , 3H, $–CH_2–CH_3$). ^{13}C NMR (101 MHz, DMSO, δ_{ppm}): 182.32, 163.12, 157.92, 153.89, 138.68, 133.71, 131.51, 131.14, 130.06, 128.82, 127.03, 123.51, 115.89, 115.46, 113.53, 109.74, 59.39, 57.46, 54.09, 53.74, 26.11, 14.34. MS m/z (ESI): calcd for $C_{30}H_{35}Cl_2N_2O^+$: 509.21; found 509.22.

3 Results and discussion

We performed fluorescence imaging on zebrafish and nude mouse tumours without needing to introduce other fluorescent tagging agents. Therefore, in contrast with aromatic *N*-mustards, fatty *N*-mustards have lysosome-targeting and antitumour activity. As a consequence, this study provides a reference for the development of novel lysosome-targeted anticancer drugs to inhibit cell proliferation in the field of innovative drug research.

We first investigated the absorbance (UV-visible) and fluorescence emission spectra of the three target compounds. As shown in Fig. S1 (cf. Electronic Supplementary Material, ESM) and Table S1 (cf. ESM), compounds **CXL118**, **CXL121**, and **CXL122** exhibited maximum fluorescence emissions at 573, 553, and 597 nm in PBS/DMSO (7/3, v/v, pH = 7.4), respectively. The maximum UV absorbances of compounds **CXL118**, **CXL121**, and **CXL122** were 450, 427, and 433 nm, respectively [40,41]. Specifically, the Stokes shift of **CXL122** was greater than 160 nm, which indicated minimized excitation interference in cell-imaging experiments. Therefore, the following studies mainly focused on compound **CXL122**.

Because of the aforementioned fluorescent properties, these compounds can be used in the cellular environment to exert effects. To determine whether **CXL118**, **CXL121**, and/or **CXL122** can specifically localize in lysosomes, HeLa cells were incubated with one of the synthetic fluorescent fatty *N*-mustards (2 $\mu mol \cdot L^{-1}$) and lysosome-tracker deep red (lysotracker deep red, a commercially available lysosome dye, 300 $nmol \cdot L^{-1}$) for 20 min [42]. Subsequently, co-localization experiments were performed using the method described. As shown in Fig. 2, after HeLa cells were incubated with these compounds, the fluorescence ascribed to **CXL118**, **CXL121**, and **CXL122** clearly co-localized with lysosomes, and the Pearson correlation coefficients were 0.84, 0.74 and 0.82, respectively. Moreover, as shown in the merged images presented in Fig. 2, we confirmed that all compounds can penetrate the cell membrane, and fluorescent signals were located only in the intracellular region.

As shown in Fig. 3, an 3-(4,5)-dimethylthiahiazo(-2)-3,5-diphenytetrazoliumromide (MTT) assay was performed to test the antiproliferative activity of the fluorescent agents (**CXL118**, **CXL121**, and **CXL122**) at gradient concentrations (0.078, 0.156, 0.313, 0.625, 1.25, 2.5, 5, 10 and 20 $\mu mol \cdot L^{-1}$) in different cell lines (A549, DU145, HeLa and BCPAP cells). The results are shown in

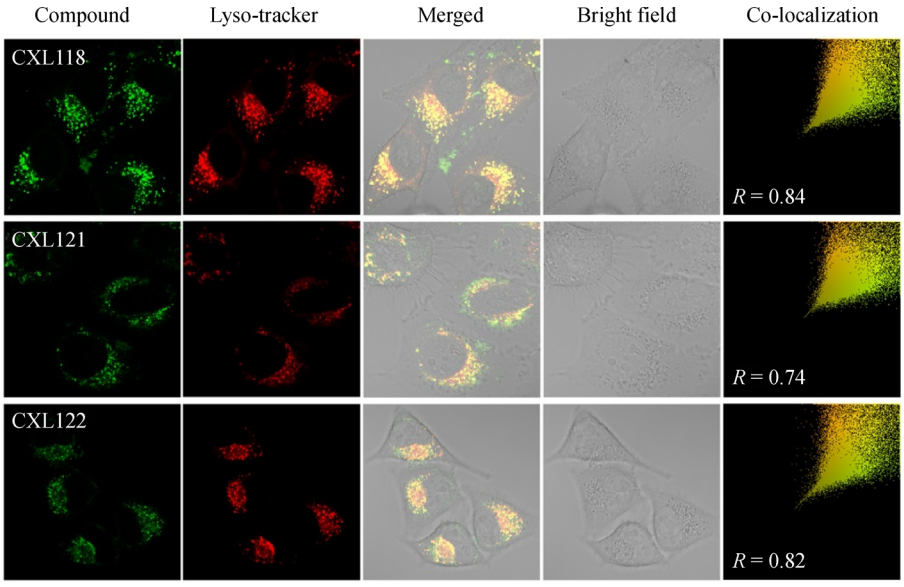

Fig. 2 HeLa cells were cultured with compounds **CXL118** (2 $\mu mol \cdot L^{-1}$), **CXL121** (2 $\mu mol \cdot L^{-1}$), and **CXL122** (2 $\mu mol \cdot L^{-1}$) and lysotracker deep red (300 $nmol \cdot L^{-1}$) for 20 min. The compounds **CXL118**, **CXL121**, and **CXL122** possess maximum UV absorption at 400–450 nm and maximum emission wavelengths between 550 and 600 nm. For these compounds, the green channel (400–520 nm), 488 nm was the excitation wavelength; for the lysotracker deep red channel (620–750 nm), 633 nm was the excitation wavelength.

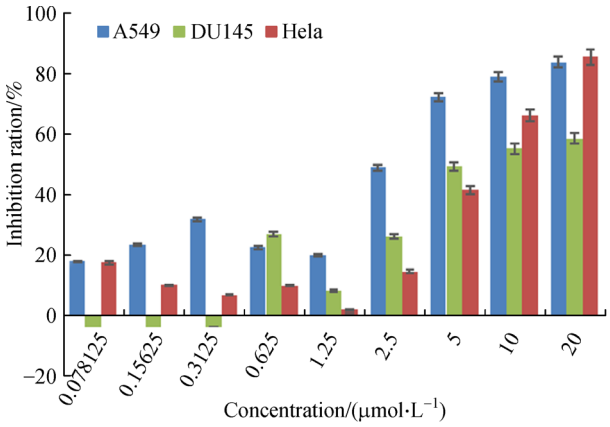

Fig. 3 MTT assay of different cell lines treated with the compounds. The inhibition rate of **CXL122** in different cells was assayed at different drug concentrations (0.078, 0.156, 0.313, 0.625, 1.25, 2.5, 5, 10, and 20 μmol·L^{-1}). The antiproliferative activity of all compounds was evaluated by MTT assay in different cell types, including A549 cells (a lung cancer cell line), DU145 cells (a human prostate cancer cell line), and HeLa cells (a cervical cancer cell line). The values represent mean ± S.D. (n = 3).

Table 1. Compounds **CXL118**, **CXL121**, and **CXL122** showed different antiproliferative activities. Overall, **CXL118**, **CXL121**, and **CXL122** have a certain inhibitory effect on A549 cells, DU145 cells, HeLa cells and BCPAP cells, with particularly potent inhibition of A549 cells.

Next, Western blot assays were performed to examine the effect of **CXL122** on the LC3-I, LC3-II, P62, and Bcl-2 protein expression in intact cells; LC3-I, LC3-II and P62 are the typical substrates evaluated in autophagy research. As shown in Fig. 4(A), the autophagy rate increased in a **CXL122** concentration-dependent manner. Furthermore, the level of P62 was lower in the **CXL122**-treated groups than in the control group. In addition, we also investigated the effects of **CXL122** on Bcl-2 protein expression in the apoptotic pathway. The results showed that **CXL122** decreased the levels of Bcl-2 in the A549 cell line in a dose-dependent manner. In addition, bis(2-chloroethyl) amine was used as a positive control to study cell death. The Western blot assays indicated a reduction in Bcl-2 protein expression with an increase in the concentration of bis(2-chloroethyl)amine, which suggested that apoptosis was the main cause of cell death. All these results suggest that **CXL122**-induced autophagy in lung cancer cells may occur simultaneously with cancer cell apoptosis.

Finally, fluorescence-assisted flow cytometry was used to study the ability of the fluorescent fatty-*N*-mustards to be taken up by A549 cells (Fig. 4(B)) [43,44]. In this experiment, no compound was added to the control group, only the commercially available stains Annexin V and PI were added (Fig. 4(B-a); (b) shows the result of adding only **CXL122** at a concentration of 10 μmol·L^{-1} without additional stain). Notably, the performance of the experimental group without any additional dye was similar to that of the experimental group in which additional dyes were added in the physiological range (Fig. S2, cf. ESM). The flow cytometry experiments illustrate that the fluorescent fatty nitrogen mustard molecules eliminated background interference and the misleading data associated with unreacted labelling dyes, which makes the analysis more efficient and economical.

Zebrafish, which have been widely used in biological and biochemical research, are important model organisms with rapid embryonic development and short generation times [45,46]. Zebrafish embryos and larvae have frequently been used for *in vivo* imaging [47]. Here, we described the results of fluorescence imaging of zebrafish using **CXL122** as the probe, which was introduced into zebrafish embryos and larvae by soaking. Green *in vivo* fluorescence imaging with **CXL122** used as a probe was observed, as shown in Fig. 5, which presents bright field and fluorescence images of embryos and larvae after soaking with **CXL122**. As shown in Fig. 5(A), the fluorescence images of embryos 3 h post-fertilization (hpf) become brighter with increasing concentrations of **CXL122**, whereas the bright field images did not differ from each other. Next, fluorescence imaging of zebrafish embryos after soaking with **CXL122** (at 2.5 μmol·L^{-1}) enabled the visualization of embryo development at different periods, namely, from the single cell stage to larval stage (Fig. 5(B)). We found that **CXL122** did not disturb embryo development, demonstrating the low toxicity and high biocompatibility of **CXL122**. Finally, zebrafish larvae were used as models to validate the results of the imaging application of **CXL122** *in vivo*. Fig. 5(C) shows whole bodies of zebrafish larvae 78 hpf after

Table 1 IC_{50} values for the synthesized compounds

Cell line	IC_{50}/(μmol·L^{-1}) [a]			
	A549	DU145	HeLa	BCPAP
CXL118	5.78 ± 1.5	7.18 ± 1.1	8.64 ± 1.3	> 20
CXL121	2.06 ± 1.1	10.28 ± 1.3	17.35 ± 1.2	> 20
CXL122	1.55 ± 1.3	7.87 ± 1.1	6.72 ± 1.4	> 40
Bis(2-chloroethyl)amine	2.78 ± 1.2	8.94 ± 1.4	11.63 ± 1.3	> 30

a) Cytotoxicity was determined by MTT assay after 72 h of treatment. The data are representative of three independent experiments.

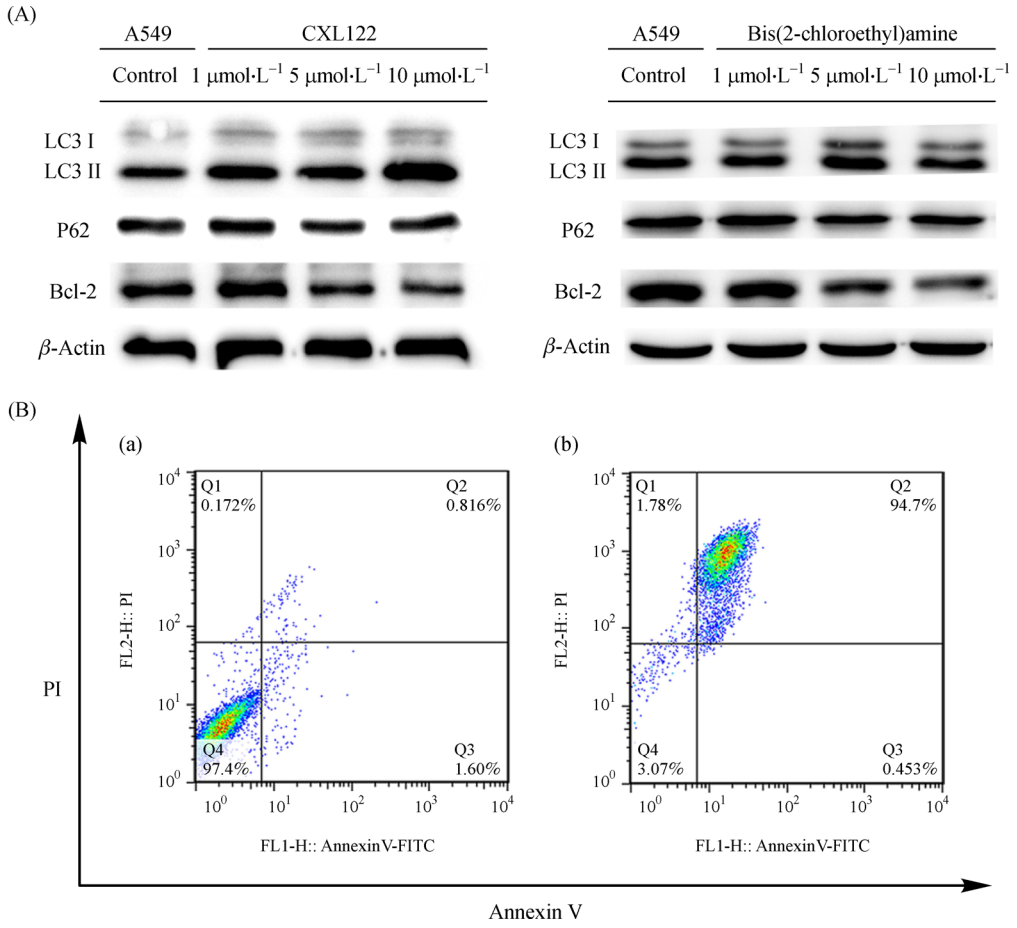

Fig. 4 (A) Western blot analysis of LC3-I, LC3-II, P62, and Bcl-2 protein expression in A549 cells treated with the indicated doses of **CXL122** and bis(2-chloroethyl)amine for 72 h; (B) Flow cytometry to evaluate the effect of **CXL122**. (a) Control with Annexin V and PI added; (b) without additional stain, i.e., only **CXL122** (10 μmol·L^{-1}) was added to cells.

soaking in **CXL122** solution at different concentrations for 6 h. The zebrafish larvae became increasingly brighter with increasing concentration, showing a concentration-dependent reaction, illustrating that **CXL122** was successfully introduced into the larvae. These results validate the practicability of using **CXL122** as an imaging probe.

Among various diagnostic imaging techniques, fluorescence imaging agents provide accurate outcomes for cancer diagnosis through non-invasive, real-time, and high-resolution imaging [48–50]. *In vivo* imaging of various fluorescent chemical compounds has been reported [51,52]. Therefore, to provide further evidence on the fluorescence imaging capacity of **CXL122** *in vivo*, dye (20 mmol·L^{-1}, 25 μL) was injected into the tumour site of nude mice bearing BxPC-3 cells and imaged at various times (0, 5, 10, 15, 20, 25 and 30 min). As depicted in Fig. 6, the fluorescence intensity within the tumour was markedly high and increased over time after the intratumour injection of **CXL122**; however, the control did not show any significant fluorescence *in vivo*. Thirty minutes after the injection, the fluorescence imaging of **CXL122** demonstrated a stronger fluorescence intensity at tumour sites than at healthy sites, attesting to the outstanding tumour imaging capacity and long-term preservation time of the probe at tumour sites.

4 Conclusions

In conclusion, we developed three novel related multifunctional fatty *N*-mustard compounds (**CXL118**, **CXL121**, and **CXL122**) that were selectively located in the lysosomes of living cells. Because of the excellent fluorescent properties of these compounds, using flow cytometry, we directly analysed the results without the need for incorporating additional dyes or stains. These fatty *N*-mustard compounds have potent antitumour with inhibitory cell proliferation activity. Zebrafish embryos and larvae were used as models to validate the practicability of using **CXL122** as an *in vivo* imaging probe. *In vivo* tumour

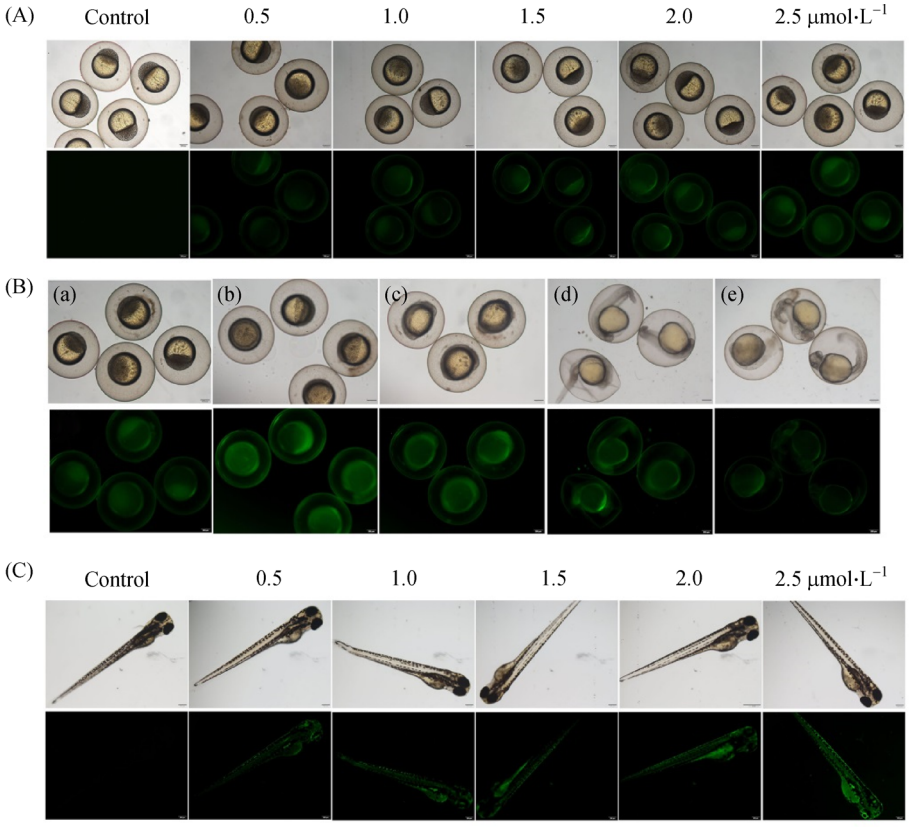

Fig. 5 Bright field and fluorescence images of zebrafish embryos and zebrafish. (A) Bright field (upper) and fluorescence (lower) images of zebrafish embryos 3 hpf after soaking for 3 h in **CXL122** solution of different concentrations (0.5, 1.0, 1.5, 2.0, and 2.5 μmol·L^{-1}). The Images acquired under bright light show the yolk sac (ys) and the inner mass of the embryos (ime). A 4× objective lens was used. Scale bars, 200 μm. (B) Bright field (upper) and fluorescence (lower) images taken at different time points of zebrafish embryos after soaking in 2.5 μmol·L^{-1}**CXL122** solution for 3 h: (a) 3, (b) 6, (c) 12, (d) 24, and (e) 48 hpf. A 4× objective lens was used. Scale bars, 200 μm. (C) Bright field (upper) and fluorescence (lower) images of the whole bodies of zebrafish larvae taken 78 hpf after soaking for 6 h in **CXL122** solution of different concentrations. A 4× objective lens was used. Scale bars, 200 μm.

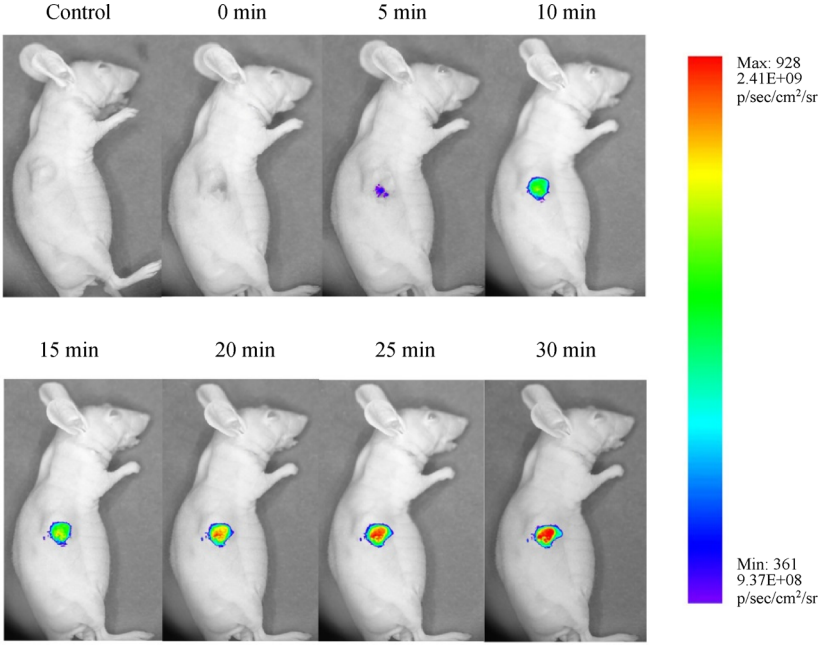

Fig. 6 Representative images of BxPC-3 tumour-bearing mice acquired at different times after intratumour injection with **CXL122** *in vivo*.

imaging in a BxPC-3 tumour-bearing mouse experiment showed that **CXL122** had outstanding tumour imaging capacity and long-term preservation time at tumour sites. We anticipate that this design concept will enable the development of additional fluorescent molecules containing fatty *N*-mustard and inspire the production of more efficient fluorescent probes for use *in vivo*.

Acknowledgements This work was financially supported by Science and Technology Department of Sichuan Province (Nos. 2020YJ0237, 2018SZ0030, 2019YFH0119), National Clinical Research Center for Geriatrics, West China Hospital, Sichuan University (Z20191006) and the 135 Project for Disciplines of Excellence, West China Hospital, Sichuan University (Nos. ZYJC18025 and ZYJC18003).

Electronic Supplementary Material Supplementary material is available in the online version of this article at https://dx.doi.org/10.1007/s11705-021-2075-5 and is accessible for authorized users.

Compliance with Ethics Guidelines Xiuli Chen, Feng Liu, Bin Chen, Haiying Wu, Kun Li, Yongmei Xie, Weihong Kuang and Zhihui Li declare that they have no conflict of interest. All institutional and national guidelines for the care and use of laboratory animals were followed.

References

1. Liu Y, Zhou J, Wang L, Hu X, Liu X, Liu M, Cao Z, Shangguan D, Tan W. A cyanine dye to probe mitophagy: simultaneous detection of mitochondria and autolysosomes in live cells. Journal of the American Chemical Society, 2016, 138(38): 12368–12374
2. Luzio J P, Pryor P R, Bright N A. Lysosomes: fusion and function. Nature Reviews. Molecular Cell Biology, 2007, 8(8): 622–632
3. Zhang H, Liu J, Liu C, Yu P, Sun M, Yan X, Guo J P, Guo W. Imaging lysosomal highly reactive oxygen species and lighting up cancer cells and tumors enabled by a Si-rhodamine-based near-infrared fluorescent probe. Biomaterials, 2017, 133: 60–69
4. Li M, Fan J, Li H, Du J, Long S, Peng X. A ratiometric fluorescence probe for lysosomal polarity. Biomaterials, 2018, 164: 98–105
5. Maiuri M, Tasdemir E, Criollo A, Morselli E, Vicencio J, Carnuccio R, Kroemer G. Control of autophagy by oncogenes and tumor suppressor genes. Cell Death and Differentiation, 2009, 16(1): 87–93
6. Mohamed M M, Sloane B F. Cysteine cathepsins: multifunctional enzymes in cancer. Nature Reviews. Cancer, 2006, 6(10): 764–775
7. Soreghan B, Thomas S N, Yang A J. Aberrant sphingomyelin/ceramide metabolic-induced neuronal endosomal/lysosomal dysfunction: potential pathological consequences in age-related neurodegeneration. Advanced Drug Delivery Reviews, 2003, 55(11): 1515–1524
8. Mizukami H, Mi Y, Wada R, Kono M, Yamashita T, Liu Y, Werth N, Sandhoff R, Sandhoff K, Proia R L. Systemic inflammation in glucocerebrosidase-deficient mice with minimal glucosylceramide storage. Journal of Clinical Investigation, 2002, 109(9): 1215–1221
9. Reiser J, Adair B, Reinheckel T. Specialized roles for cysteine cathepsins in health and disease. Journal of Clinical Investigation, 2010, 120(10): 3421–3431
10. Vasiljeva O, Reinheckel T, Peters C, Turk D, Turk V, Turk B. Emerging roles of cysteine cathepsins in disease and their potential as drug targets. Current Pharmaceutical Design, 2007, 13(4): 387–403
11. Miao R, Li M, Zhang Q, Yang C, Wang X. An ECM-to-nucleus signalling pathway activates lysosomes for *C. elegans* larval development. Developmental Cell, 2020, 52(1): 21–37
12. Fujimaki K, Li R, Chen H, Croce K D, Zhang H H, Xing J, Bai F, Yao G. Graded regulation of cellular quiescence depth between proliferation and senescence by a lysosomal dimmer switch. Proceedings of the National Academy of Sciences of the United States of America, 2019, 116(45): 22624–22634
13. Hu R, Chen B, Wang Z, Qin A, Zhao Z, Lou X, Tang B Z. Intriguing "chameleon" fluorescent bioprobes for the visualization of lipid droplet-lysosome interplay. Biomaterials, 2019, 203: 43–51
14. Fan J, Dong H, Hu M, Wang J, Zhang H, Zhu H, Sun W, Peng X. Fluorescence imaging lysosomal changes during cell division and apoptosis observed using Nile blue based near-infrared emission. Chemical Communications, 2013, 50(7): 882–884
15. Kroemer G, Jäättelä M. Lysosomes and autophagy in cell death control. Nature Reviews. Cancer, 2005, 5(11): 886–897
16. Chen J W, Pan W, D'souza M P, August J T. Lysosome-associated membrane proteins: characterization of LAMP-1 of macrophage P388 and mouse embryo 3T3 cultured cells. Archives of Biochemistry and Biophysics, 1985, 239(2): 574–586
17. Werneburg N W, Guicciardi M E, Bronk S F, Kaufmann S H, Gores G J. Tumor necrosis factor-related apoptosis-inducing ligand activates a lysosomal pathway of apoptosis that is regulated by bcl-2 proteins. Journal of Biological Chemistry, 2007, 282(39): 28960–28970
18. Hu Q, Bally M B, Madden T D. Subcellular trafficking of antisense oligonucleotides and down-regulation of bcl-2 gene expression in human melanoma cells using a fusogenic liposome delivery system. Nucleic Acids Research, 2002, 30(16): 3632–3641
19. Hanaki K, Momo A, Oku T, Komoto A, Maenosono S, Yamaguchi Y, Yamamoto K. Semiconductor quantum dot/albumin complex is a long-life and highly photostable endosome marker. Biochemical and Biophysical Research Communications, 2003, 302(3): 496–501
20. Hotchkiss R S, Strasser A, McDunn J E, Swanson P E. Cell death. New England Journal of Medicine, 2009, 361(16): 1570–1583
21. Kroemer G, El-Deiry W S, Golstein P, Peter M E, Vaux D, Vandenabeele P, Zhivotovsky B, Blagosklonny M V, Malorni W, Knight R A, et al. Classification of cell death: recommendations of the nomenclature committee on cell death. Cell Death and Differentiation, 2005, 12(S2): 1463–1467
22. Galluzzi L, Maiuri M, Vitale I, Zischka H, Castedo M, Zitvogel L, Kroemer G. Cell death modalities: classification and pathophysiological implications. Cell Death and Differentiation, 2007, 14(7): 1237–1243
23. Walls K C, Ghosh A P, Franklin A V, Klocke B J, Ballestas M, Shacka J J, Zhang J, Roth K A. Lysosome dysfunction triggers Atg7-dependent neural apoptosis. Journal of Biological Chemistry, 2010, 285(14): 10497–10507
24. Codogno P, Meijer A J. Atg5: more than an autophagy factor. Nature Cell Biology, 2006, 8(10): 1045–1047
25. Yu T, Guo F, Yu Y, Sun T, Ma D, Han J, Qian Y, Kryczek I, Sun D, Nagarsheth N, et al. Fusobacterium nucleatum promotes chemore-

sistance to colorectal cancer by modulating autophagy. Cell, 2017, 170(3): 548–563
26. Amaravadi R K, Thompson C B. The roles of therapy-induced autophagy and necrosis in cancer treatment. Clinical Cancer Research, 2007, 13(24): 7271–7279
27. Marx J. Autophagy: is it cancer's friend or foe? Science, 2006, 312 (5777): 1160–1161
28. Giralt S, Thall P F, Khouri I, Wang X, Braunschweig I, Ippolitti C, Claxton D, Donato M, Bruton J, Cohen A, et al. Melphalan and purine analog-containing preparative regimens: reduced-intensity conditioning for patients with hematologic malignancies undergoing allogeneic progenitor cell transplantation. Blood, 2001, 97(3): 631–637
29. Pedersen P J, Christensen M S, Ruysschaert T, Linderoth L, Andresen T L, Melander F, Mouritsen O G, Madsen R, Clausen M H. Synthesis and biophysical characterization of chlorambucil anticancer ether lipid prodrugs. Journal of Medicinal Chemistry, 2009, 52(10): 3408–3415
30. Li W, Nie S, Chen Y, Wang Y, Li C, Xie M. Enhancement of cyclophosphamide-induced antitumor effect by a novel polysaccharide from Ganoderma atrum in sarcoma 180-bearing mice. Journal of Agricultural and Food Chemistry, 2011, 59(8): 3707–3716
31. Chen W, Balakrishnan K, Kuang Y, Han Y, Fu M, Gandhi V, Peng X. Reactive oxygen species (ROS) inducible DNA cross-linking agents and their effect on cancer cells and normal lymphocytes. Journal of Medicinal Chemistry, 2014, 57(11): 4498–4510
32. Verwilst P, Han J, Lee J, Mun S, Kang H G, Kim J S. Reconsidering azobenzene as a component of small-molecule hypoxia-mediated cancer drugs: a theranostic case study. Biomaterials, 2017, 115: 104–114
33. Detroja D, Chen T L, Lin Y W, Yen T Y, Wu M H, Tsai T H, Mehariya K, Kakadiya R, Lee T C, Shah A. Novel *N*-mustard-benzimidazoles/benzothiazoles, synthesis and anticancer evaluation. Anti-cancer Agents in Medicinal Chemistry, 2017, 17: 1741–1755
34. Diethelm-Varela B, Ai Y, Liang D, Xue F. Nitrogen mustards as anticancer chemotherapies: historic perspective, current developments and future trends. Current Topics in Medicinal Chemistry, 2019, 19(9): 691–712
35. Singh R K, Prasad D N, Bhardwaj T R. Hybrid pharmacophore-based drug design, synthesis, and antiproliferative activity of 1,4-dihydropyridines-linked alkylating anticancer agents. Medicinal Chemistry Research, 2015, 24(4): 1534–1545
36. Chen X, Chen H, Lu C, Yang C, Yu X, Li K, Xie Y. Novel mitochondria-targeted, nitrogen mustard-based DNA alkylation agents with near infrared fluorescence emission. Talanta, 2016, 161: 888–893
37. Chen X, Peng W, Huang S, Yang C, Hu M, Yang S, Yang S, Xie Y, Chen H, Lei N, Luo Y, Li K. Novel mitochondria-targeted and fluorescent DNA alkylation agents with highly selective activity against cancer cells. Dyes and Pigments, 2019, 170: 107610
38. Tang L, He P, Yan X, Sun J, Zhong K, Hou S, Bian Y. A mitochondria-targetable fluorescent probe for ratiometric detection of SO_2 derivatives and its application in live cell imaging. Sensors and Actuators. B, Chemical, 2017, 247: 421–427
39. Zhou Q, Li K, Liu Y H, Li L L, Yu K K, Zhang H, Yu X Q. Fluorescent Wittig reagent as a novel ratiometric probe for the quantification of 5-formyluracil and its application in cell imaging. Chemical Communications, 2018, 54(97): 13722–13725
40. Wu M Y, Li K, Li C Y, Hou J T, Yu X Q. A water-soluble near-infrared probe for colorimetric and ratiometric sensing of SO_2 derivatives in living cells. Chemical Communications, 2014, 50(2): 183–185
41. Liu Y, Li K, Wu M Y, Liu Y H, Xie Y M, Yu X Q. A mitochondria-targeted colorimetric and ratiometric fluorescent probe for biological SO_2 derivatives in living cells. Chemical Communications, 2015, 51 (50): 10236–10239
42. Li D P, Wang Z Y, Cao X J, Cui J, Wang X, Cui H Z, Miao J Y, Zhao B X. A mitochondria-targeted fluorescent probe for ratiometric detection of endogenous sulfur dioxide derivatives in cancer cells. Chemical Communications, 2016, 52(13): 2760–2763
43. Puckett C A, Barton J K. Methods to explore cellular uptake of ruthenium complexes. Journal of the American Chemical Society, 2007, 129(1): 46–47
44. Li Y, Tao L, Zuo Z, Zhou Y, Qian X, Lin Y, Jie H, Liu C, Li Z, Zhang H, et al. ZY0511, a novel, potent and selective LSD1 inhibitor, exhibits anticancer activity against solid tumors via the DDIT4/mTOR pathway. Cancer Letters, 2019, 454: 179–190
45. Ko S K, Chen X, Yoon J, Shin I. Zebrafish as a good vertebrate model for molecular imaging using fluorescent probes. Chemical Society Reviews, 2011, 40(5): 2120–2130
46. Deniz Koç N, Yüce R. A light-and electron microscopic study of primordial germ cells in the zebra fish (*Danio rerio*). Biological Research, 2012, 45(4): 331–336
47. Kang Y F, Li Y H, Fang Y W, Xu Y, Wei X M, Yin X B. Carbon quantum dots for zebrafish fluorescence imaging. Scientific Reports, 2005, 5(1): 11835
48. Liang D, Zhang Y, Wu Z, Chen Y J, Yang X, Sun M, Ni R, Bian J, Huang D. A near infrared singlet oxygen probe and its applications in in vivo imaging and measurement of singlet oxygen quenching activity of flavonoids. Sensors and Actuators. B, Chemical, 2018, 266: 645–654
49. Ding F, Zhan Y, Lu X, Sun Y. Recent advances in near-infrared II fluorophores for multifunctional biomedical imaging. Chemical Science (Cambridge), 2018, 9(19): 4370–4380
50. Han X, Wang R, Song X, Yu F, Chen L. Evaluation selenocysteine protective effect in carbon disulfide induced hepatitis with a mitochondrial targeting ratiometric near-infrared fluorescent probe. Analytical Chemistry, 2018, 90(13): 8108–8115
51. Hu M, Yang C, Luo Y, Chen F, Yang F, Yang S, Chen H, Cheng Z, Li K, Xie Y. A hypoxia-specific and mitochondria-targeted anticancer theranostic agent with high selectivity for cancer cells. Journal of Materials Chemistry. B, Materials for Biology and Medicine, 2018, 6(16): 2413–2416
52. Qu X, Yuan F, He Z, Mai Y, Gao J, Li X, Yang D, Cao Y, Li X, Yuan Z. A rhodamine-based single-molecular theranostic agent for multiple-functionality tumor therapy. Dyes and Pigments, 2019, 166: 72–83